No.: egusphere-2023-2913

Title: Measurement Report: Elevated excess-NH_3 can promote the redox reaction to produce HONO: Insights from the COVID-19 pandemic

Reviewer #1:

General Comments:

In this study, the authors analyzed the chemical composition changes during the pandemic in ten urban and rural sites, and compared the HONO concentration level before and during the emission control period. The authors found that the HONO decline was relatively insignificant compared to its precursors and a detailed calculation shows that the enhanced production rate of aqueous phase reaction partially offset the effect of lower precursors. By comparing the atmospheric acids and bases concentrations, the authors suggested that the enhanced level of NH_3 and elevated aerosol pH due to less acidic components in the atmosphere was the reason for the higher HONO production rate. It can be one of the possible reasons, while there are several important issues that the authors did not have enough discussion or provide clear explanation. Some analysis and explanations are too simplified to give the assessment of the quality of this study.

Thank you for your careful reading of our paper and valuable comments and

suggestions. We believe that we have adequately addressed your comments. To facilitate your review, we used yellow highlights for your comments, green highlights for Reviewer #2, and red color indicating our own corrections in the manuscript.

Major issues:

1. The direct emission HONO was estimated based on the vehicle emission factors and NO_x concentration level, which should reflect a general situation of normal human activities. However, during the pandemic, the emission factors could change very significantly if only necessary activities were allowed to be carried out. The authors did not mention emission profile change before and during the pandemic, which could lead to the overestimation of the effect of other pathways.

Response: Thanks for your comments. We determined whether it is necessary to calculate vehicle emissions, and a supplementary HONO emission factor table from vehicle emissions was added to support the selection of factors in the revised version:

"HONO can be released directly into the atmosphere through vehicle exhaust (Burling et al., 2010; Veres et al., 2010). The lifetime of HONO in the atmosphere is relatively short, so vehicle emissions significantly contribute to urban atmospheric HONO (Chen et al., 2023; Liu et al., 2021a). Considering that there has been a significant reduction in vehicle emissions in urban areas during DC. Additionally, the R-PY site is far from roads. Thus, vehicle emissions may not be the primary source of HONO for the U-ZK site during DC and R-PY sites during entire periods. To further

validate the above conclusions, the conditional bivariate probability function diagrams of NO_2 at U-ZK and R-PY sites during PC and DC are depicted in Figure S2. NO_2 predominantly originated from long-distance transport at the U-ZK site during DC and the R-PY site during both PC and DC. Consequently, vehicle emissions are only calculated for the U-ZK site during the PC.

Here we use the HONO/NO_x ratio to estimate HONO concentration, which is generally considered to be the vehicle emission factor (Kramer et al., 2020; Hao et al., 2020; Yu et al., 2022) for HONO. The calculation formula is as follows：

$$[HONO_{emi}] = 0.8\% \times [NO_x] \quad (1)$$

where [$HONO_{emi}$] and [NO_x] represent the HONO concentration emitted by vehicles and the observed NO_x concentration, respectively. Regarding previous studies (Table S3), 0.8% was selected as the vehicle emission factor, considering differences in vehicle type, fuel composition, and other factors (Kramer et al., 2020; Hao et al., 2020; Huang et al., 2017).”

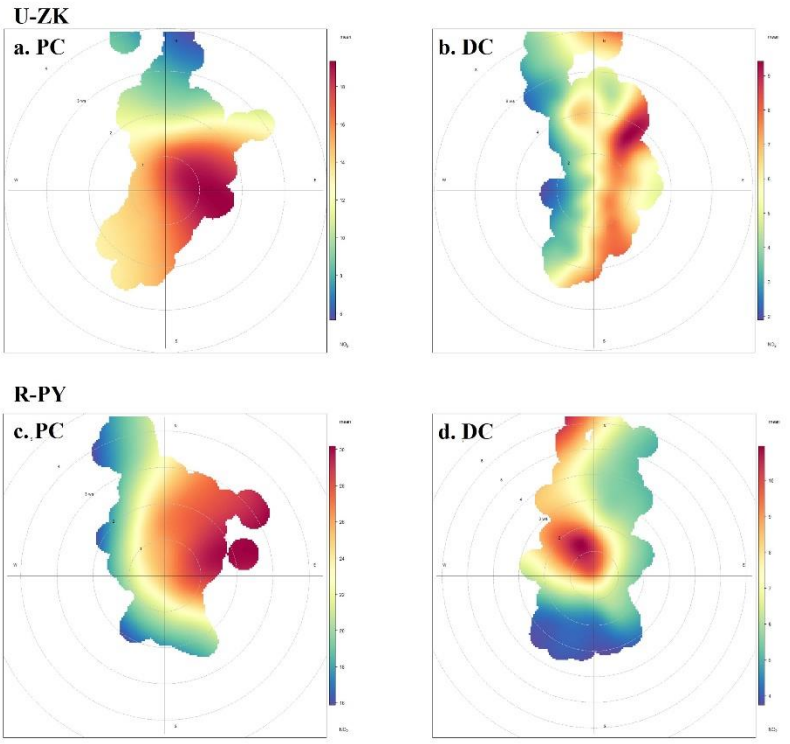

Figure S2. Result of conditional bivariate probability function plots: NO_2 at U-ZK and R-PY sites before (PC) and during (DC) the COVID-19 outbreak. The color scale bar represents NO_2 concentration.

Table S3. Summary of vehicle emission factors.

Observation site	Period	Emission factor (%)	Reference
Beijing	2020	0.79	(Meng et al., 2020)
Hong Kong	2015	0.4–1.8	(Yun et al., 2017)
Hong Kong	2011	0.5–1.6	(Xu et al., 2015)
Kiesberg Tunnel	2001	0.8	(Kleffmann et al., 2003)
Kiesberg Tunnel	1997	0.3–0.8	(Kurtenbach and Wiesen, 2001)
Guangzhou	2019	1.31	(Li et al., 2021b)

2. Supplement Line 107: it is very challenging to pick a representative OH concentration to represent the general situation. The authors also suggested in the

introduction that OH radical concentration could change during emission control as part of atmospheric oxidizing capacity changes. While the authors did not mention such an approach in their HONO production calculation. In addition to other reaction pathways, another possibility is the change of reaction rates, like OH concentration levels and higher temperature (the authors only mentioned H and K temperature dependence but did not mention k_1 temperature dependence, which could be important). The authors should fully discuss the possibilities of the changes in reaction rate and possible sinks.

Response: Thank you for your valuable comments.

Firstly, we have modified the method for determining •OH concentration in the revised manuscript:

"•OH concentration was simulated according to the empirical model (Hu et al., 2022; Wang et al., 2025):

$$[OH] = 4.1\times10^{9} \times \frac{J(O^{1}D)\times J(NO_2)\times(140\times[NO_2]+1)+[HONO]\times J(HONO)}{0.41\times[NO_2]^2+1.7\times[NO_2]+1+[NO]\times k_{NO+OH}+[HONO]\times k_{NO+OH}} \quad (12)$$

where, J (O^1 D), J (NO_2), and J (HONO) are the photolysis rates calculated using the TUV model (v5.2; available at http://cprm.acom.ucar.edu/Models/TUV/). The calculated •OH concentration varied from 0.1 × 10^6 to 4 × 10^6 molecule/cm^3 at U-ZK and 0.1 × 10^6 to 5 × 10^6 molecule/cm^3 t R-PY, which was comparable to the levels in other cities of North China (Li et al., 2018; Fuchs et al., 2017; Yang et al., 2017). Since there is no photolysis at night, the •OH concentration was assumed to be 0.8 × 10^6 molecule/cm^3 (Wang et al., 2022)."

Secondly, the sources of HONO were recalculated to better investigate the changes

in HONO between PC and DC periods:

Text S4 Sources of HONO

4.1 Direct emission

HONO can be released directly into the atmosphere through vehicle exhaust (Burling et al., 2010; Veres et al., 2010). The lifetime of HONO in the atmosphere is relatively short, so vehicle emissions significantly contribute to urban atmospheric HONO (Chen et al., 2023; Liu et al., 2021a). Considering that there has been a significant reduction in vehicle emissions in urban areas during DC. Additionally, the R-PY site is far from roads. Thus, vehicle emissions may not be the primary source of HONO for the U-ZK site during DC and R-PY sites during entire periods. To further validate the above conclusions, the conditional bivariate probability function diagrams of NO_2 at U-ZK and R-PY sites during PC and DC are depicted in Figure S2. NO_2 predominantly originated from long-distance transport at the U-ZK site during DC and the R-PY site during both PC and DC. Consequently, vehicle emissions are only calculated for the U-ZK site during the PC.

Here we use the HONO/NO_x ratio to estimate HONO concentration, which is generally considered to be the vehicle emission factor (Kramer et al., 2020; Hao et al., 2020; Yu et al., 2022) for HONO. The calculation formula is as follows：

$$[HONO_{emi}] = 0.8\% \times [NO_x] \quad (1)$$

where [$HONO_{emi}$] and [NO_x] represent the HONO concentration emitted by vehicles

and the observed NO_x concentration, respectively. Regarding previous studies (Table S3), 0.8% was selected as the vehicle emission factor, considering differences in vehicle type, fuel composition, and other factors (Kramer et al., 2020; Hao et al., 2020; Huang et al., 2017).

4.2 Homogeneous reaction of NO and •OH

The reaction between NO and •OH is the primary gas-phase reaction source of HONO at high NO concentrations, and the production rate contribution (P_{OH+NO}) for this reaction can be calculated as:

$$P_{OH+NO} = k_{OH+NO}[OH][NO] \quad (2)$$

where k_{OH+NO} (7.2×10^{-12} cm^3 $molecule^{-1}$ s^{-1}) is the rate constant for the reactions at 298K (Li et al., 2012). •OH concentration was simulated according to the empirical model (Hu et al., 2022; Wang et al., 2025):

$$[OH] = 4.1\times10^{9} \times \frac{J(O^1D)\times J(NO_2)\times(140\times[NO_2]+1)+[HONO]\times J(HONO)}{0.41\times[NO_2]^2+1.7\times[NO_2]+1+[NO]\times k_{NO+OH}+[HONO]\times k_{NO+OH}} \quad (3)$$

where, J (O^1 D), J (NO_2), and J (HONO) are the photolysis rates calculated using the TUV model (v5.2; available at http://cprm.acom.ucar.edu/Models/TUV/). The cloud optical depth value for the TUV model was adjusted so that the predicted UVB radiation intensity matched the observations (Lyu et al., 2019; Wang et al., 2022b). The calculated •OH concentration varied from 0.1×10^6 to 4×10^6 molecule/cm^3 at U-ZK and 0.1×10^6 to 5×10^6 molecule/cm^3 t R-PY, which was comparable to the levels in other cities of North China (Li et al., 2018; Fuchs et al., 2017; Yang et al., 2017). Since there is no

photolysis at night, the •OH concentration was assumed to be 0.8×10^6 molecule/cm^3 (Wang et al., 2022).

4.3 Heterogeneous conversion of NO_2 to HONO

4.3.1 Heterogeneous dark reactions

The heterogeneous conversion of NO_2 to HONO on the ground (P_{ground}) and on the aerosol surface ($P_{aerosol}$) was calculated based on parameters obtained from experiments or observations.

$$P_{ground} = \frac{1}{8}\gamma_1 \times [NO_2] \times C_{NO_2} \times \frac{S_g}{V} \quad (4)$$

$$P_{aerosol} = \frac{1}{4}\gamma_2 \times [NO_2] \times C_{NO_2} \times \frac{S_a}{V} \quad (5)$$

$$\frac{S_g}{V} = \frac{1}{MLH} \quad (6)$$

$$C_{NO_2} = \sqrt{\frac{8RT}{\pi M}} \quad (7)$$

where C_{NO2} is the average molecular velocity of NO_2 molecule (m s^{-1}); R is the ideal gas constant; T is the temperature (K); M is the molecular weight of NO_2 (kg mol^{-1}); MLH is the height of the mixed layer, which is determined to be 50 m due to HONO formation on the ground level and its short lifetime (Liu et al., 2020b); S_a/V is the surface area to volume ratio of aerosol, estimated by Su et al. (Su et al., 2008).

4.3.2 Heterogeneous photo-enhanced reactions

The heterogeneous photo-enhanced reactions of NO_2 on the surface of the ground

($P_{ground+hv}$) and the surface of the aerosol ($P_{aerosol+hv}$) were calculated following (Zhang et al., 2020a):

$$P_{ground+hv} = \frac{1}{8} \times C_{NO_2} \times \frac{1}{MLH} \times \gamma_1 \times \frac{J_{NO_2}}{J_{NO_{2,noon}}} \times [NO_2] \quad (8)$$

$$P_{aerosol+hv} = \frac{1}{4} \times C_{NO_2} \times \frac{S_a}{V} \times \gamma_2 \times \frac{J_{NO_2}}{J_{NO_{2,noon}}} \times [NO_2] \quad (9)$$

where JNO_2 and $JNO_{2,\,noon}$ are the photolysis rate of NO_2 and the photolysis rate of NO_2 at noon during the day, respectively.

γ_1 and γ_2 are the absorption coefficient of NO_2 on the ground and aerosol surface, respectively, which is assumed to be 4×10^{-6} (Yu et al., 2022; Zhang et al., 2021; Zhang et al., 2020a). Moreover, we discuss the uncertainties based on the recommended values of 2×10^{-6}–1×10^{-5} as upper and lower bounds(Chen et al., 2023; VandenBoer et al., 2013; Wong et al., 2011). Results show (Figure S3) that the uncertainties for P_{ground}, $P_{aerosol}$, $P_{groung+hv}$, and $P_{aerosol+hv}$ are −50% to 150%, −50% to 151%, −20% to 120%, and −50% to 121% at the U-ZK, respectively. At the R-PY, the uncertainties for P_{ground}, $P_{aerosol}$, $P_{groung+hv}$, and $P_{aerosol+hv}$ are −50% to 150%, −50% to 151%, −20% to 120%, and −50% to 121%, respectively.

4.4 Nitrate photolysis

The nitrate photolysis ($P_{nitrate}$) was calculated based on the measured nitrate concentration (NO_3^-) from $PM_{2.5}$ and nitrate photolysis rate ($J_{nitrate\rightarrow HONO}$):

$$P_{nitrate} = J_{nitrate\rightarrow HONO} \times [NO_3^-] \quad (10)$$

where the $J_{nitrate \rightarrow HONO}$ was simulated by normalizing UV values, when the Zenit Angle is 0°, $J_{nitrate \rightarrow HONO}$ varied within the range of 1.22×10^{-5} to 4.84×10^{-4} s^{-1}, with an average value of 8.24×10^{-5} s^{-1} (Bao et al., 2018)."

Unfortunately, for MLH, S_a/V, and the relationship between k1 and temperature, as there were no observational data or scientifically established estimation methods, this study did not consider their variations. This omission may lead to differences in conclusions and warrants further investigation in future research.

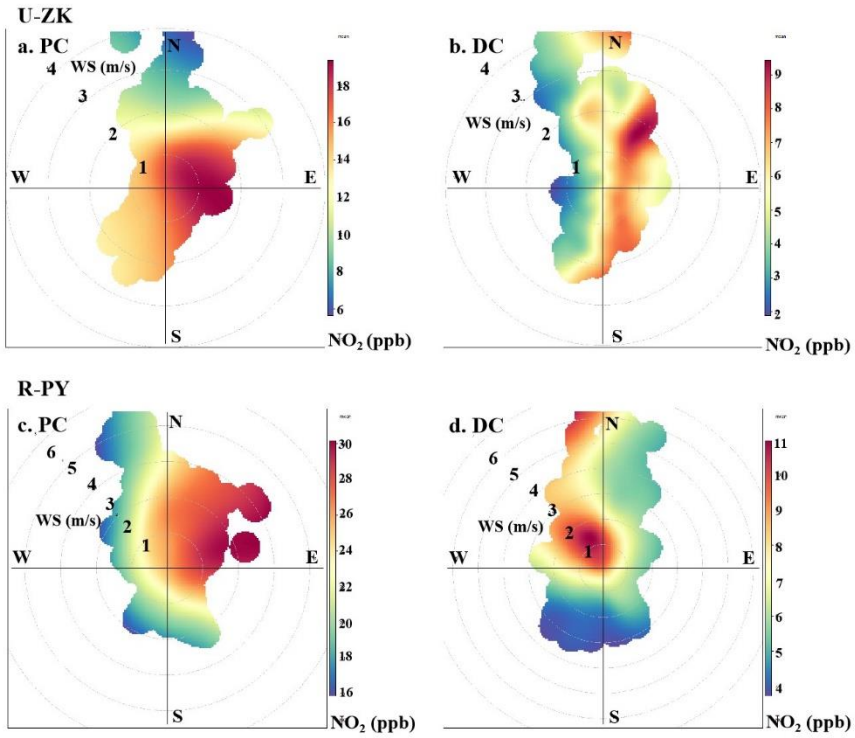

Figure S2. Result of conditional bivariate probability function plots: NO_2 at U-ZK and R-PY sites before (PC) and during (DC) the COVID-19 outbreak. The color scale bar represents NO_2 concentration.

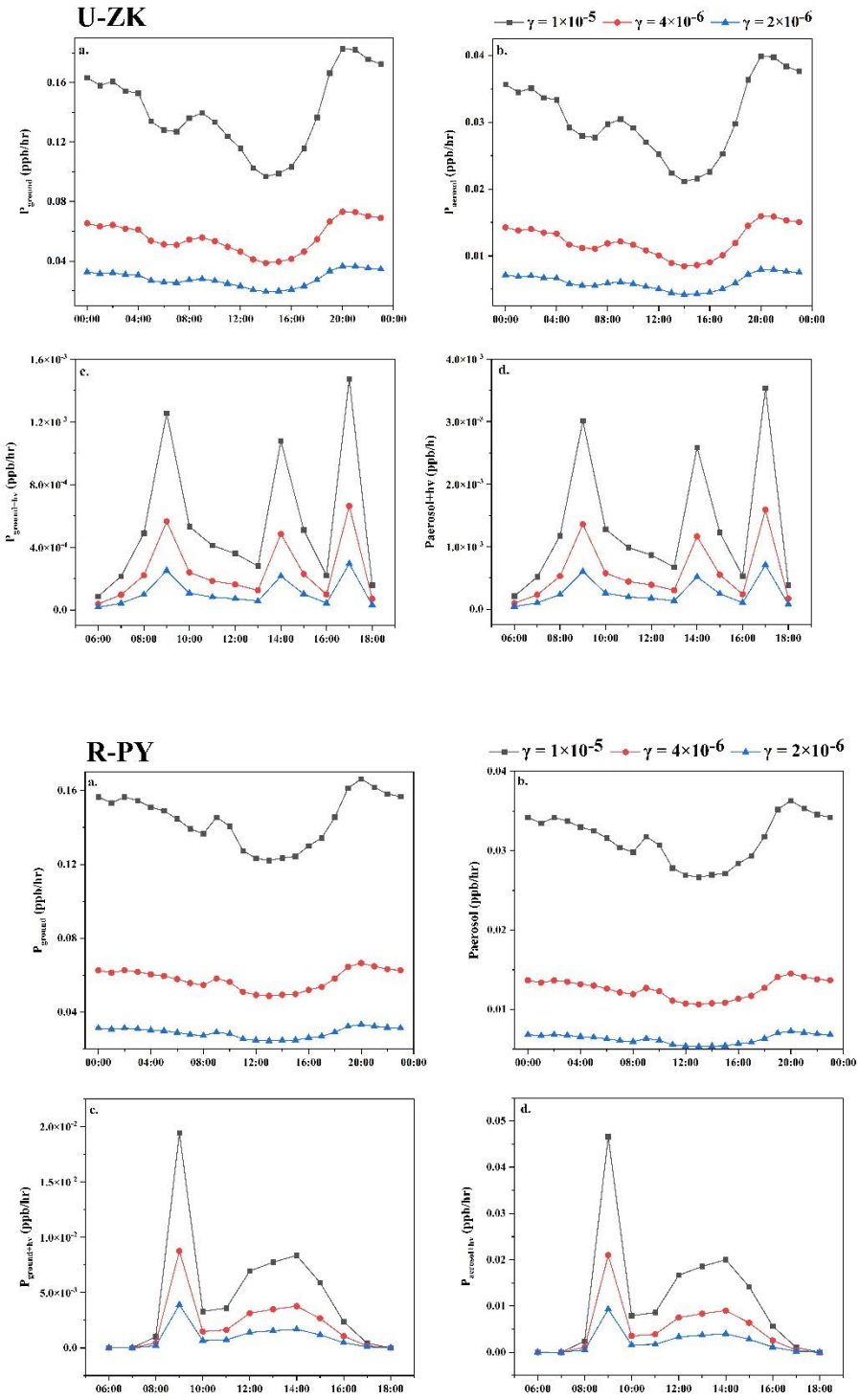

Figure S3. HONO production rate using different uptake rates of NO_2 at the U-ZK and R-PY sites before (PC) and during (DC) the COVID-19 outbreak. (a)P_{ground}, (b) $P_{aerosol}$, (c) $P_{ground+hv}$, and (d) $P_{aerosol+hv}$

Table S3. Summary of vehicle emission factors.

Observation site	Period	Emission factor (%)	Reference
Beijing	2020	0.79	(Meng et al., 2020)
Hong Kong	2015	0.4–1.8	(Yun et al., 2017)
Hong Kong	2011	0.5–1.6	(Xu et al., 2015)
Kiesberg Tunnel	2001	0.8	(Kleffmann et al., 2003)
Kiesberg Tunnel	1997	0.3–0.8	(Kurtenbach and Wiesen, 2001)
Guangzhou	2019	1.31	(Li et al., 2021b)

3. It is also questionable about the contribution of NH_3 concentration changes to the total pH changes. Temperature, relative humidity, and other salts could also contribute to pH changes. It was not mentioned how the sensitivity tests of Line 264-275 were done and the interpretation of the results was also unclear. The authors did not give a complete pH comparison like NH_x levels, only provided two sites in Figure 4. The authors mentioned the increase of pH 0.4 and 0.1 for U-ZK and R-PY sites respectively. However, based on the NH_3 levels shown in Table 1 and the relationship mentioned in Song et al. (2019): $\partial pHi/\partial[NH_3(g)] \approx 0.4/[NH_3(g)]$, the NH_3 concentration changes was only responsible for 0.13-unit pH change in U-ZK (less than half). The pH changes of most sites, if only considering NH_3 levels changes in Table 1, can be calculated to be around 0.1 with the exception of R-SQ where NH_3 concentration nearly doubled.

Response: Sorry for the misunderstanding. The formula in Song's study only considers the effect of NH_3 on the pH value of particulate matter and does not take into account other substances such as TH_2SO_4, TNO_3, T, etc., which have a greater impact on pH value. Therefore, when the NH_3 value in this study is brought into the formula, there is

a different conclusion obtained. To explore the dominant factors that determine the high pH during the DC, we have added a detailed description of the sensitivity tests of pH to input data:

"To explore the dominant factors that determine the local particle pH level and result in the high pH during the DC, sensitivity tests of pH to chemical species (i.e., TNH_x, TH_2SO_4, TNO_3, TCl, TNa, K^+, Ca^{2+}, and Mg^{2+}) and meteorological parameters (i.e., To explore the dominant factors that determine the local particle pH level and result in the high pH during the DC, sensitivity tests of pH to chemical species (i.e., TNH_x, TH_2SO_4, TNO_3, TCl, TNa, K^+, Ca^{2+}, and Mg^{2+}) and meteorological parameters (i.e., T and RH) were performed. A given range for a variable (i.e., TNH_x) with corresponding average values of other parameters (i.e., TH_2SO_4, TNO_3, TCl, TNa, K^+, Ca^{2+}, Mg^{2+}, T, and RH) was input into the model and simulated to compare its effects on pH. As shown in Fig. S7, pH increases with the cation concentrations (i.e., TNH_x, Na^+, K^+, Ca^{2+}, and Mg^{2+}) increasing as well as the anion concentrations (i.e., TH_2SO_4, TNO_3, and Cl^-), T and RH decreasing. According to the average values of input data during PC (Blue line in Fig. S7) and DC (Red line in Fig. S7) at U-ZK and R-PY sites respectively, the changes in pH (ΔpH in Fig. 5) indicate that the decrease in TNH_x concentration and the increase in T in DC led to a decrease in pH values (ΔpH: 0.09 at U-ZK and 0.08 at R-PY sites) compared to PC. However, this effect was outweighed by the decrease in TH_2SO_4 (ΔpH: 0.07 and 0.8 at U-ZK and R-PY sites, respectively) and TNO_3 (ΔpH: 0.05 and 0.4 at U-ZK and R-PY sites, respectively) concentrations as well as the increase in K^+ (ΔpH:

0.03 at U-ZK and 0.2 at R-PY site) and Mg^{2+} (ΔpH: 0.01 at U-ZK and 0.04 at R-PY site) concentrations in the DC, and resulting in an overall increase in pH values in the DC. Furthermore, the relationship between particle pH with the concentrations of Required-NH_x, and Excess-NH_x, which considers all chemical components, is investigated to examine the dominant factor on the increasing pH in DC. As shown in Fig. 6, the higher Excess-NH_x concentrations in the DC led to higher increases in pH values (ΔpH: 1 at U-ZK and 0.5 at R-PY site) than those in PC (ΔpH: 0.3 at U-ZK and 0.2 at R-PY site), thus Excess-NHx concentrations may be the key factor in promoting the pH values."

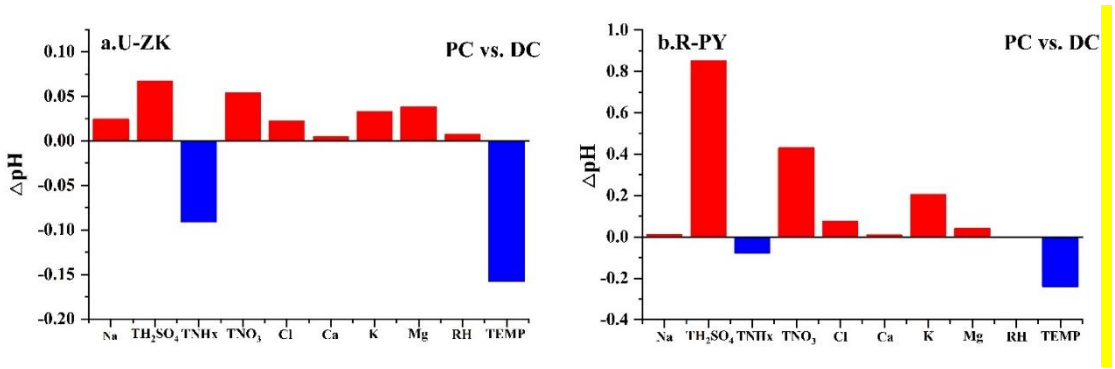

Figure 5. Changes of pH (ΔpH) through the sensitivity tests (Figure S5 and S6) by changing parameters between PC and DC at the a. U-ZK and b. R-PY sites.

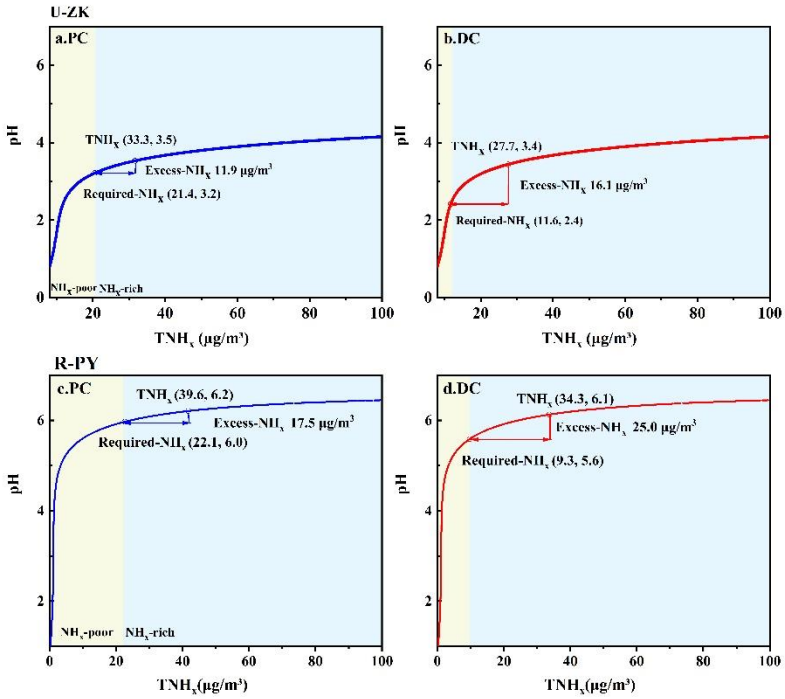

Figure 6. Particle pH corresponds to increasing TNH_x at U-ZK and R-PY sites to examine the effects of major indicators of NH_3 (i.e., TNH_x, Required-NH_x, and Excess-NH_x) on aerosol acidity. Particle pH was calculated by using a wide range of TNH_x (25–130 μg/m^3) and average values of other parameters in PC and DC of U-ZK and R-PY sites. The concentrations of TNH_x, Required-NH_x, and Excess-NH_x with corresponding pH values are marked by a hollow box, hollow circle, and arrow respectively. The yellow and blue background colors correspond to the NH_x-poor and NH_x-rich, respectively.

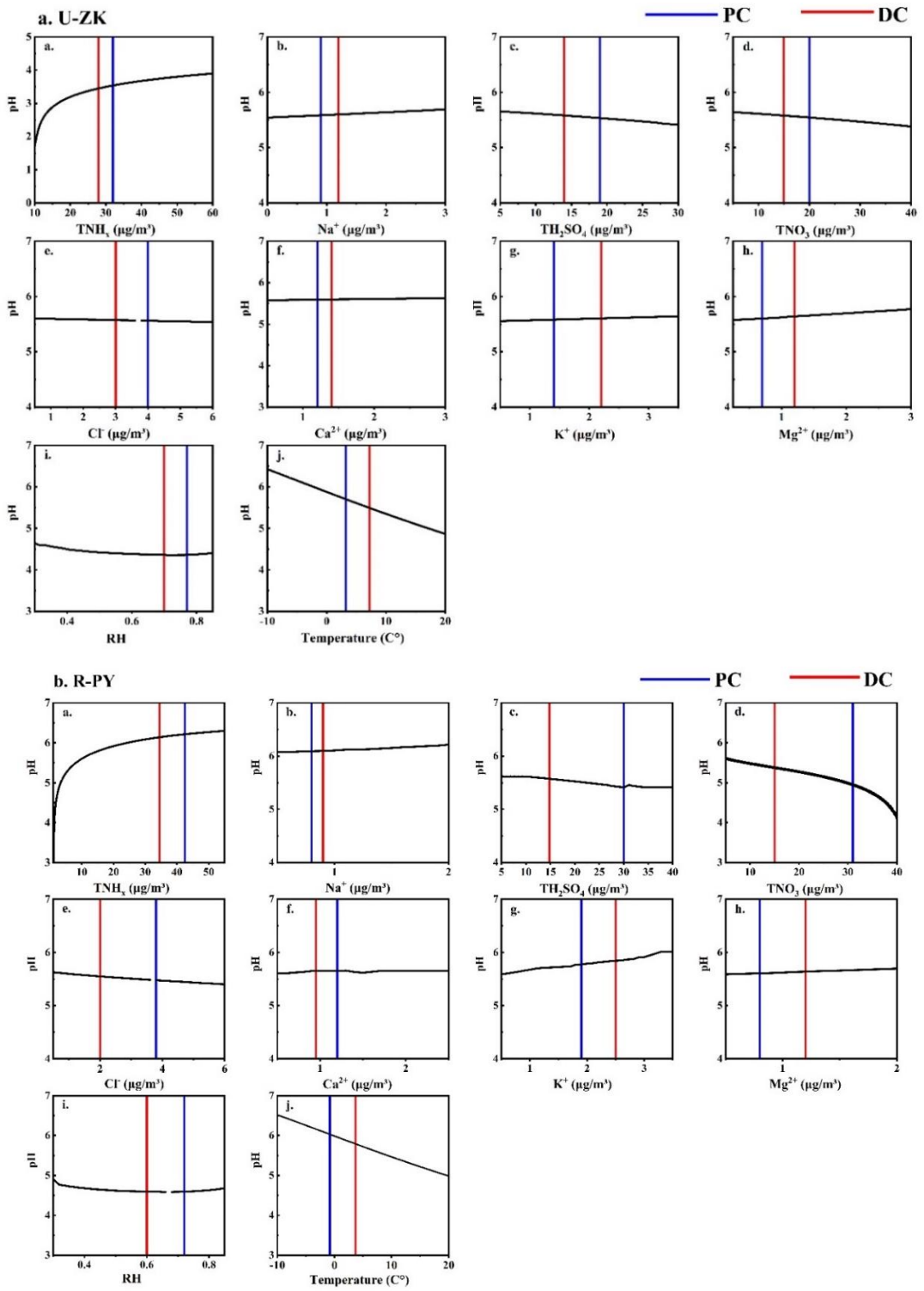

Figure S7. Sensitivity tests of pH to each factor. The vertical bar represents the mean values before (PC) and during (DC) the COVID-19 outbreak. A given range for a variable (i.e., TNH_x) with corresponding average values of other parameters (i.e., TH_2SO_4, TNO_3, TCl, TNa, K^+, Ca^{2+}, Mg^{2+}, T, and RH) was simulated to compare its effects on pH.

Additionally, we have added a complete pH comparison of ten sites:

"Diurnal patterns of particle pH in PC and DC at ten sites are summarized in Fig. 4 with their average values listed in Table S9. $PM_{2.5}$ shows consistent moderate acidity, with mean values in the range of 4.2–5.1, which were close to the values in previous studies (Table S9). Compared to the PC, the particle pH at ten sites increased obviously in the DC, with the highest increase of 0.5 (U-ZK) and 0.3 (R-PY) at urban and rural sites, respectively, which were the subject of in-depth discussion in the following text."

.

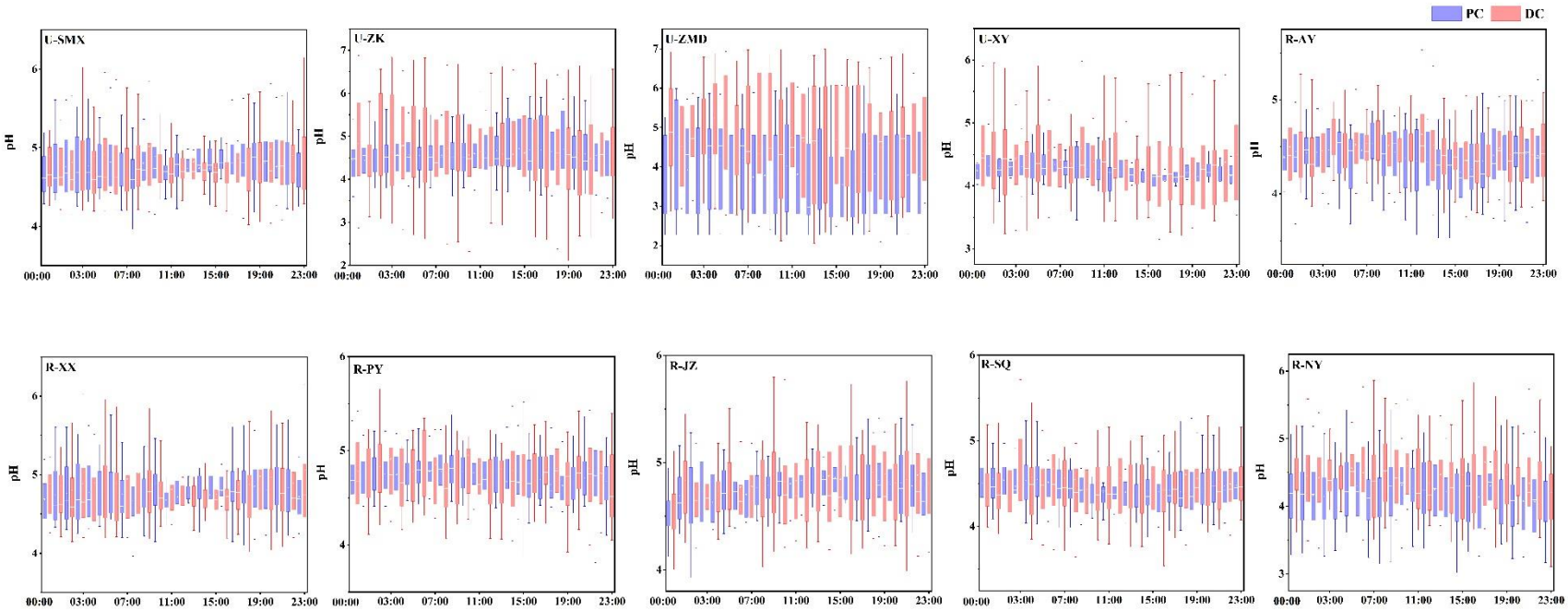

Figure 4. Diurnal patterns of pH at ten sites before (PC) and during (DC) the COVID-19 outbreak. In each box, the top, middle, and bottom lines represent the 75, 50, and 25 percentiles of statistical data, respectively; the upper and lower whiskers represent the 90 and 10 percentiles of statistical data, respectively

Table S9. Comparison of the particle pH values in this study (PC/DC) and other sites (mean or mean ± standard).

	Sites	Periods	pH	References
Urban	Sanmenxia	Jan–Feb 2020	4.6 ± 0.5/4.8 ± 0.9	This study
	Zhoukou	Jan–Feb 2020	4.6 ± 0.6/5.1 ± 0.4	
	Zhumadian	Jan–Feb 2020	4.6 ± 0.3/4.8 ± 1.2	
	Xinyang	Jan–Feb 2020	4.2 ± 0.3/4.6 ± 1.3	
Rural	Anyang	Jan–Feb 2020	4.5 ± 0.4/4.6 ± 0.8	
	Xinxiang	Jan–Feb 2020	4.8 ± 0.5/4.9 ± 0.9	
	Puyang	Jan–Feb 2020	4.8 ± 0.3/5.1 ± 0.9	
	Jiaozuo	Jan–Feb 2020	4.9 ± 0.5/5.1 ± 0.8	
	Shangqiu	Jan–Feb 2020	4.5 ± 0.3/4.7 ± 0.8	
	Nanyang	Jan–Feb 2020	4.2 ± 0.5/4.4 ± 0.7	
Urban	Beijing	Jan–Feb 2015	4.5	(Guo et al., 2017)
	Beijing	Dec 2016	4.3 ± 0.4	(Liu et al., 2017)
	Beijing	Feb 2017	4.5 ± 0.7	(Ding et al., 2019)
	Tianjin	Dec–Jun 2015	4.9 ± 1.4	(Shi et al., 2017)
	Tianjin	Aug 2015	3.4 ± 0.5	(Shi et al., 2019)
	Hohhot	Winter	5.7	(Wang et al., 2019)
	Mt. Tai	Summer	2.9 ± 0.5	(Liu et al., 2021b)
	Taoyuan	Nov 2017–Jan 2018	5.1 ± 1.0	(Duan et al., 2021)
	Zhengzhou	Jan 2018	4.5	(Wang et al., 2020)
	Anyang	Jan 2018	4.8	(Wang et al., 2020)
Mountain	Mt. Tai	Summer	3.6 ± 0.7	(Liu et al., 2021b)
Rural	Shanglan	Nov 2017–Jan 2018	5.5 ± 1.1	(Duan et al., 2021)

4. Figure 4, the maximum and minimum values provided little information of the whole pH variations. A box and whisker plot are more useful to identify the general trends and variations. And there were frequent situations of maximum pH higher than 7, which could not be explained by higher NH_3 concentrations. Instead, it could be from the strong influence of dust components. If that situation happened frequently enough (hard to judge now based on the information given), it could be the dust components that are actually responsible for the high pH.

Response: Thank you for your suggestions. We redrew Figure 4 as a box diagram and replaced it in the revised version. After examining the raw data, we found that the pH data higher than 7 mainly concentrated in clean air with low pollutant concentrations. Additionally, some data had RH levels below 30%, which could lead to significant errors in the model. Thus, ISORROPIA-II was rerun only using data with RH ≥ 30% in the revised version.

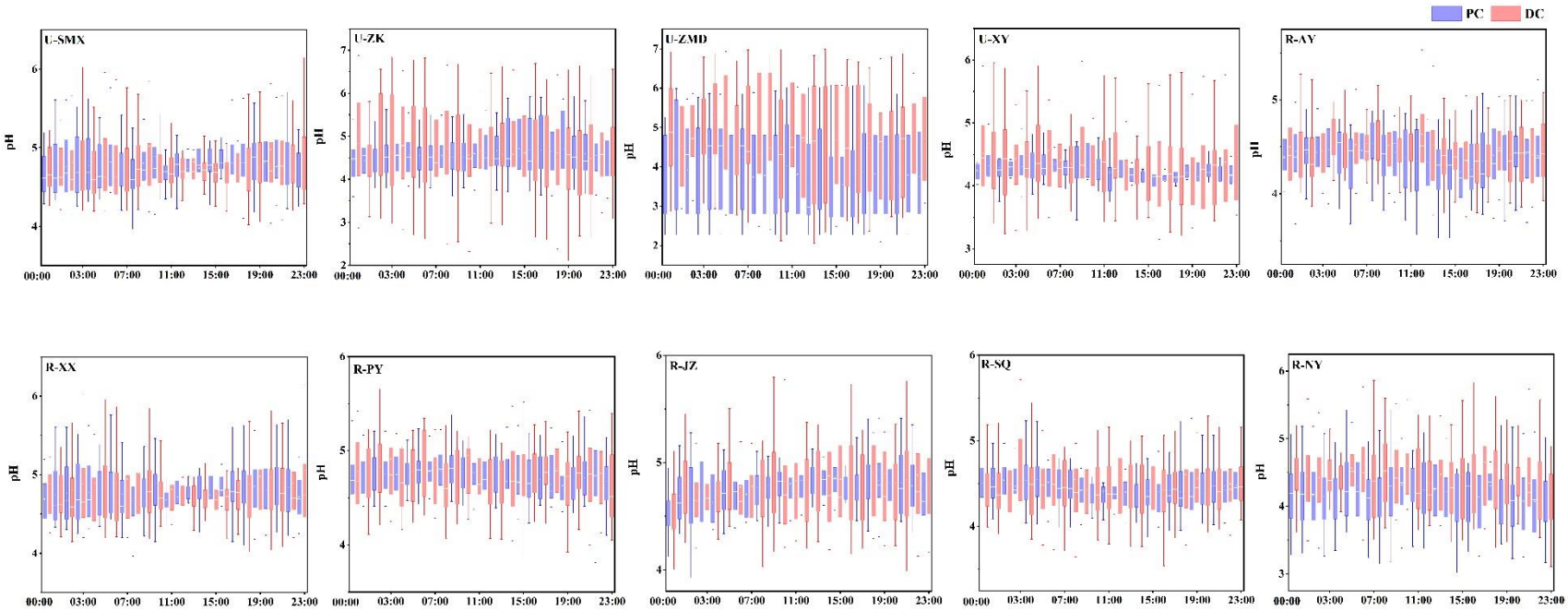

Figure 4. Diurnal patterns of pH at ten sites before (PC) and during (DC) the COVID-19 outbreak. In each box, the top, middle, and bottom lines represent the 75, 50, and 25 percentiles of statistical data, respectively; the upper and lower whiskers represent the 90 and 10 percentiles of statistical data, respectively.

5. It should also be mentioned that the approach of the authors used to estimate AWC_{org} is sensitive to the parameters chosen, such as OM/OC ratio, density, and kappa parameter. Normally, the term AWC_{org} is small enough so that its influence is limited, while it is possible the uncertainty associated with the parameters chosen became big enough when inorganic salts become depleted and the relative contribution of OM got enhanced.

Response: Thank you for your comment. We supplemented the selection criteria for calculating parameters in the revised manuscript:

"AWC_{org} is the particle water associated with the organic matters predicted using the following method:

$$AWC_{org} = \frac{m_s}{\rho_s} \frac{k_{org}}{\left(\frac{1}{RH} - 1\right)} \quad (2.2)$$

where m_s is the mass concentration of organic matter (OM = OC × f). The f is the conversion factor of OC, which is dependent on the extent of OM oxidation and secondary organic aerosol formation (Chow et al., 2015). Studies on the ratio of OM/OC in fourteen cities in China suggested that the mean value of f was 1.59 ± 0.18 during the winter season in Northern China (Xing et al., 2013), and thus we adopted 1.6 as the f in this study. k_{org} is the organic hygroscopicity parameter and depends on organic functionality, water solubility, molecular weight, and oxidation level. Han et al. (2022) have reported that the k_{org} generally increased with O: C ratios, with a range of 0–0.3 for 23 organics, including carboxylic acids, amino acids, sugars, and alcohols. Gunthe

et al, (2011) estimated a k_{org} = 0.06 ± 0.01 for the effective average hygroscopicity of the non-refractory organic particulate matter in the aerosols in Beijing. Our previous study has estimated that the uncertainties of k_{org} value (0.06) for pH in the range of 0–0.3 only lead to –1–3% errors, which can be neglected (Wang et al., 2023a). Therefore, the value of 0.06 was selected in this paper. ρ_s is the organic density, which was chosen to be 1.35 g/cm^3 following previous studies (Table S2)."

Table S2. The value of ρ_s in other studies.

Observation site	Period	ρ_s (g/cm^3)	Reference
Beijing	Dec 2016	1.4	(Liu et al., 2017)
Tianjin	Dec-Jun 2015	1.3	(Shi et al., 2017)
Xi'an	Nov-Dec 2012	1.4	(Guo et al., 2017)
Hohhot	Winter 2015	1.35	(Wang et al., 2019)
Northeastern USA	Feb-Mar 2015	1.4	(Guo et al., 2016)
Crete, Greece	Aug-Nov 2012	1.35	(Bougiatioti et al., 2016)
Alabama, USA	Jun-Jul 2013	1.4	(Guo et al., 2015)
Georgia, USA	Aug-Oct 2016	1.4	(Nah et al., 2018)

Minor issues:

6. The definition of TNHx is different in Line113 and Line 228.

Response: Thank you for your careful reading of our paper. The formula is used uniformly in the new version:

$$TNH_x = 17 \times \left(\frac{[NH_4^+]}{18} + \frac{[NH_3]}{17}\right)$$

7. Line 42, the study cited is the result based on a field campaign.

Response: Thank you for your comment. We added more references: "Nitrous acid (HONO) is a critical precursor of hydroxyl radical (OH), contributing to more than 60%

of OH production (Alicke, 2003; Platt et al., 1980; Kleffmann et al., 2005)."

8. Figure 2, the max and min as error bars provide little information about the general trends, and there are negative values.

Response: Thank you for your comments. We redrew Figure 2 as a box diagram and the negative values were removed after quality control.

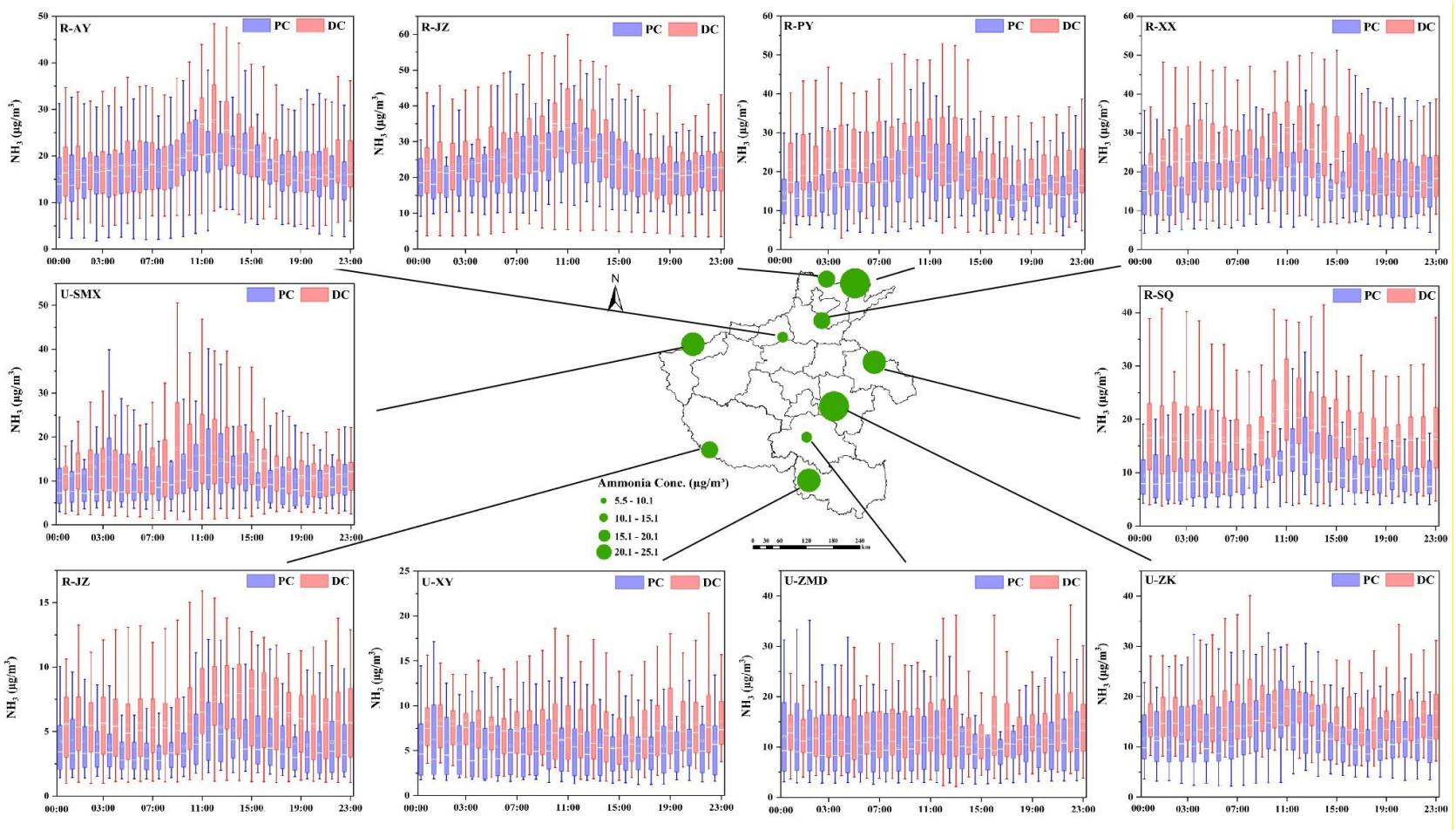

Figure 2. Daily variation of NH_3 concentration at ten sites before (PC) and during (DC) the COVID-19 outbreak. The green dots represent the location of ten sites and their size represents the concentration of NH_3; In each box, the top, middle, and bottom lines represent the 75, 50, and 25 percentiles of statistical data, respectively; the upper and lower whiskers represent the 90 and 10 percentiles of statistical data, respectively.

9. Line 215, it is hard to judge if agricultural activity got weakened or not. The NH_3 concentration change could be due to less farm activity like less frequent animal feces cleaning, relatively higher temperature or a different regional transportation pattern.

Response: Thank you for your valuable suggestions. We have removed the speculation.

Reviewer #2:

General Comments:

This study reported that there was a noticeable increase in NH_3 concentrations during the COVID-19 pandemic. In addition to the meteorological conditions, the significant decrease in sulfate and nitrate concentrations enhanced the portioning of NH_4^+ to NH_3, which enables enhanced particle pH values and in turn accelerate the redox reactions between NO_2 and SO_2 to form HONO. The article has several major issues and should be considered carefully.

Thank you for your careful reading of our paper and valuable comments and suggestions. We believe that we have adequately addressed your comments. To facilitate your review, we used green highlights for your comments, yellow highlights for Reviewer #1, and red color indicating our own corrections in the manuscript.

1. In the introduction, the author comments that the exact relationship between NO_x, NH_3 and AOC remains unclear. However, it's a lengthy description of the changes in NH_3 and pH before and during the epidemic and there is no detailed discussion on the specific impact on AOC. In short, the research problems pointed out in the introduction have not been fully explored in the study, and many conclusions are very far-fetched.

Response: Thanks for your comment. In the original article, we indeed overly extended the perspectives of this study. In the revised manuscript, we removed all descriptions regarding AOC and focused on the sources of HONO, for example:

"Nitrous acid (HONO) is a critical precursor of hydroxyl radical (OH), contributing to

more than 60% of OH production (Alicke, 2003; Platt et al., 1980; Kleffmann et al., 2005). The OH can react with carbon monoxide, nitrogen oxides (NO_x), sulfur dioxide (SO_2), and volatile organic compounds to produce secondary pollutants such as ozone (O_3) and $PM_{2.5}$ (particulate matter with an aerodynamic diameter less than or equal to 2.5 μm), thereby affecting air quality, human health, and global climate change (Li et al., 2021a; Wang et al., 2023b; Lu et al., 2018)."

2. In lines 296-297, the paper argues that HONO has other sources and that the process of NO_2 reacting with SO_2 to generate HONO is currently insufficient evidence. In addition, this reaction is affected by pH, so how much does this contribution to HONO affect atmospheric oxidation? This discussion is also sorely lacking.

Response: Thanks for your comment. In recent years, an increasing number of laboratory and field observation studies have shown that the reaction of NO_2 and SO_2 can generate HONO, especially under high ammonia conditions (Ge et al., 20219; Li et al., 2018; Zhang et al., 2023, 2024). Accordingly, this study found that observed NH_3 concentrations increased during the epidemic control period, and calculated pH values showed an increase. In addition, the positive correlations between HONO with SO_2, Excess-NH_x, SO_4^{2-}, and pH further indicate the existence of reaction of NO_2 and SO_2. Moreover, we calculated the reaction rate of NO_2 and SO_2 and found that it rose by more than 50%. Although the majority of HONO unknown sources remain unexplained, this partly explains the significant decrease in NO_x during the epidemic period, but the relatively low decrease in HONO concentrations.

Ge, S., Wang, G., Zhang, S., Li, D., and Zhang, H.: Abundant NH_3 in China enhances atmospheric HONO production by promoting the heterogeneous reaction of SO_2 with NO_2. Environ. Sci. Technol. 53, 14339 – 14347, https://doi.org/10.1021/acs.est.9b04196, 2019.

Li, L., Hoffmann, M. R., and Colussi, A. J.: Role of nitrogen dioxide in the production of sulfate during Chinese haze-aerosol episodes, Environ. Sci. Technol., 52, 2686 – 2693, https://doi.org/10.1021/acs.est.7b05222, 2018.

Zhang, X., Tong, S., Jia, C., Zhang, W., Wang, Z., Tang, G., Hu, B., Liu, Z., Wang, L., Zhao, P., Pan, Y., and Ge, M.: Elucidating HONO formation mechanism and its essential contribution to OH during haze events., npj. ClWim. Atmos. Sci., 6, 55, https://doi.org/10.1038/s41612-023-00371-w, 2023.

Zhang, P., Li, H., Ma, Q., Chen, T., Chu, B., Yu, Y., and He, H.: SO_2 photoaging enhances the surface conversion of NO_2-to-HONO on elemental carbon, Environ. Sci. Technol. Lett., 11, 143 – 149, https://doi.org/10.1021/acs.estlett.3c00878, 2024.

3. About HONO sources calculation, there are also many issues. The emission of motor vehicles at different stations varies greatly, so it is unreasonable to use 0.65% as the emission factor of HONO at all stations.

Response: Thanks for your comments.

Firstly, We determined whether it is necessary to calculate vehicle emissions, and a supplementary HONO emission factor table from vehicle emissions was added to support the selection of factors in the revised version:

"HONO can be released directly into the atmosphere through vehicle exhaust (Burling et al., 2010; Veres et al., 2010). The lifetime of HONO in the atmosphere is relatively short, so vehicle emissions significantly contribute to urban atmospheric HONO (Chen et al., 2023; Liu et al., 2021a). Considering that there has been a

significant reduction in vehicle emissions in urban areas during DC. Additionally, the R-PY site is far from roads. Thus, vehicle emissions may not be the primary source of HONO for the U-ZK site during DC and R-PY sites during entire periods. To further validate the above conclusions, the conditional bivariate probability function diagrams of NO_2 at U-ZK and R-PY sites during PC and DC are depicted in Figure S2. NO_2 predominantly originated from long-distance transport at the U-ZK site during DC and the R-PY site during both PC and DC. Consequently, vehicle emissions are only calculated for the U-ZK site during the PC.

Here we use the $HONO/NO_x$ ratio to estimate HONO concentration, which is generally considered to be the vehicle emission factor (Kramer et al., 2020; Hao et al., 2020; Yu et al., 2022) for HONO. The calculation formula is as follows：

$$[HONO_{emi}] = 0.8\% \times [NO_x] \quad (1)$$

where $[HONO_{emi}]$ and $[NO_x]$ represent the HONO concentration emitted by vehicles and the observed NO_x concentration, respectively. Regarding previous studies (Table S3), 0.8% was selected as the vehicle emission factor, considering differences in vehicle type, fuel composition, and other factors (Kramer et al., 2020; Hao et al., 2020; Huang et al., 2017).”

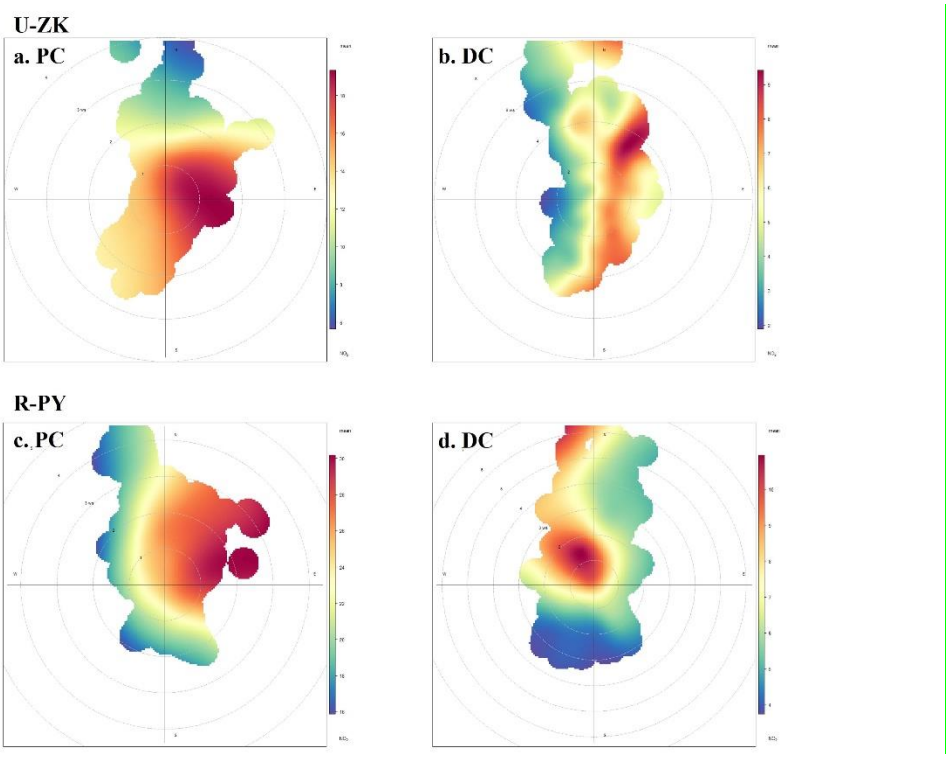

Figure S2. Result of conditional bivariate probability function plots: NO_2 at U-ZK and R-PY sites before (PC) and during (DC) the COVID-19 outbreak. The color scale bar represents NO_2 concentration.

Table S3. Summary of vehicle emission factors.

Observation site	Period	Emission factor (%)	Reference
Beijing	2020	0.79	(Meng et al., 2020)
Hong Kong	2015	0.4–1.8	(Yun et al., 2017)
Hong Kong	2011	0.5–1.6	(Xu et al., 2015)
Kiesberg Tunnel	2001	0.8	(Kleffmann et al., 2003)
Kiesberg Tunnel	1997	0.3–0.8	(Kurtenbach and Wiesen, 2001)
Guangzhou	2019	1.31	(Li et al., 2021b)

Secondly, the sources of HONO were recalculated to better investigate the changes in HONO between PC and DC periods:

Text S4 Sources of HONO

4.1 Direct emission

HONO can be released directly into the atmosphere through vehicle exhaust (Burling et al., 2010; Veres et al., 2010). The lifetime of HONO in the atmosphere is relatively short, so vehicle emissions significantly contribute to urban atmospheric HONO (Chen et al., 2023; Liu et al., 2021a). Considering that there has been a significant reduction in vehicle emissions in urban areas during DC. Additionally, the R-PY site is far from roads. Thus, vehicle emissions may not be the primary source of HONO for the U-ZK site during DC and R-PY sites during entire periods. To further validate the above conclusions, the conditional bivariate probability function diagrams of NO_2 at U-ZK and R-PY sites during PC and DC are depicted in Figure S2. NO_2 predominantly originated from long-distance transport at the U-ZK site during DC and the R-PY site during both PC and DC. Consequently, vehicle emissions are only calculated for the U-ZK site during the PC.

Here we use the $HONO/NO_x$ ratio to estimate HONO concentration, which is generally considered to be the vehicle emission factor (Kramer et al., 2020; Hao et al., 2020; Yu et al., 2022) for HONO. The calculation formula is as follows：

$$[HONO_{emi}] = 0.8\% \times [NO_x] \quad (1)$$

where $[HONO_{emi}]$ and $[NO_x]$ represent the HONO concentration emitted by vehicles and the observed NO_x concentration, respectively. Regarding previous studies (Table S3), 0.8% was selected as the vehicle emission factor, considering differences in vehicle

type, fuel composition, and other factors (Kramer et al., 2020; Hao et al., 2020; Huang et al., 2017).

4.2 Homogeneous reaction of NO and •OH

The reaction between NO and •OH is the primary gas-phase reaction source of HONO at high NO concentrations, and the production rate contribution (P_{OH+NO}) for this reaction can be calculated as:

$$P_{OH+NO} = k_{OH+NO}[OH][NO] \quad (2)$$

where k_{OH+NO} (7.2×10^{-12} cm^3 $molecule^{-1}$ s^{-1}) is the rate constant for the reactions at 298K (Li et al., 2012). •OH concentration was simulated according to the empirical model (Hu et al., 2022; Wang et al., 2025):

$$[OH] = 4.1\times10^{9} \times \frac{J(O^1D)\times J(NO_2)\times(140\times[NO_2]+1)+[HONO]\times J(HONO)}{0.41\times[NO_2]^2+1.7\times[NO_2]+1+[NO]\times k_{NO+OH}+[HONO]\times k_{NO+OH}} \quad (3)$$

where, J (O^1 D), J (NO_2), and J (HONO) are the photolysis rates calculated using the TUV model (v5.2; available at http://cprm.acom.ucar.edu/Models/TUV/). The cloud optical depth value for the TUV model was adjusted so that the predicted UVB radiation intensity matched the observations (Lyu et al., 2019; Wang et al., 2022b). The calculated •OH concentration varied from 0.1×10^6 to 4×10^6 molecule/cm^3 at U-ZK and 0.1×10^6 to 5×10^6 molecule/cm^3 t R-PY, which was comparable to the levels in other cities of North China (Li et al., 2018; Fuchs et al., 2017; Yang et al., 2017). Since there is no photolysis at night, the •OH concentration was assumed to be 0.8×10^6 molecule/cm^3 (Wang et al., 2022).

4.3 Heterogeneous conversion of NO_2 to HONO

4.3.1 Heterogeneous dark reactions

The heterogeneous conversion of NO_2 to HONO on the ground (P_{ground}) and on the aerosol surface ($P_{aerosol}$) was calculated based on parameters obtained from experiments or observations.

$$P_{ground} = \frac{1}{8}\gamma_1 \times [NO_2] \times C_{NO_2} \times \frac{S_g}{V} \quad (4)$$

$$P_{aerosol} = \frac{1}{4}\gamma_2 \times [NO_2] \times C_{NO_2} \times \frac{S_a}{V} \quad (5)$$

$$\frac{S_g}{V} = \frac{1}{MLH} \quad (6)$$

$$C_{NO_2} = \sqrt{\frac{8RT}{\pi M}} \quad (7)$$

where C_{NO2} is the average molecular velocity of NO_2 molecule (m s^{-1}); R is the ideal gas constant; T is the temperature (K); M is the molecular weight of NO_2 (kg mol^{-1}); MLH is the height of the mixed layer, which is determined to be 50 m due to HONO formation on the ground level and its short lifetime (Liu et al., 2020b); S_a/V is the surface area to volume ratio of aerosol, estimated by Su et al. (Su et al., 2008).

4.3.2 Heterogeneous photo-enhanced reactions

The heterogeneous photo-enhanced reactions of NO_2 on the surface of the ground ($P_{ground + hv}$) and the surface of the aerosol ($P_{aerosol + hv}$) were calculated following (Zhang et al., 2020a):

$$P_{ground+hv} = \frac{1}{8} \times C_{NO_2} \times \frac{1}{MLH} \times \gamma_1 \times \frac{J_{NO_2}}{J_{NO_2,noon}} \times [NO_2] \quad (8)$$

$$P_{aerosol+hv} = \frac{1}{4} \times C_{NO_2} \times \frac{S_a}{V} \times \gamma_2 \times \frac{J_{NO_2}}{J_{NO_2,noon}} \times [NO_2] \quad (9)$$

where JNO_2 and $JNO_{2,\,noon}$ are the photolysis rate of NO_2 and the photolysis rate of NO_2 at noon during the day, respectively.

γ_1 and γ_2 are the absorption coefficient of NO_2 on the ground and aerosol surface, respectively, which is assumed to be 4×10^{-6} (Yu et al., 2022; Zhang et al., 2021; Zhang et al., 2020a). Moreover, we discuss the uncertainties based on the recommended values of 2×10^{-6}–1×10^{-5} as upper and lower bounds(Chen et al., 2023; VandenBoer et al., 2013; Wong et al., 2011). Results show (Figure S3) that the uncertainties for P_{ground}, $P_{aerosol}$, $P_{groung+hv}$, and $P_{aerosol+hv}$ are −50% to 150%, −50% to 151%, −20% to 120%, and −50% to 121% at the U-ZK, respectively. At the R-PY, the uncertainties for P_{ground}, $P_{aerosol}$, $P_{groung+hv}$, and $P_{aerosol+hv}$ are −50% to 150%, −50% to 151%, −20% to 120%, and −50% to 121%, respectively.

4.4 Nitrate photolysis

The nitrate photolysis ($P_{nitrate}$) was calculated based on the measured nitrate concentration (NO_3^-) from $PM_{2.5}$ and nitrate photolysis rate ($J_{nitrate\rightarrow HONO}$):

$$P_{nitrate} = J_{nitrate\rightarrow HONO} \times [NO_3^-] \quad (10)$$

where the $J_{nitrate\rightarrow HONO}$ was simulated by normalizing UV values, when the Zenit Angle is 0°, $J_{nitrate\rightarrow HONO}$ varied within the range of 1.22×10^{-5} to 4.84×10^{-4} s^{-1}, with an average value of 8.24×10^{-5} s^{-1} (Bao et al., 2018).”

Unfortunately, for MLH, S_a/V, and the relationship between k1 and temperature, as there were no observational data or scientifically established estimation methods, this study did not consider their variations. This omission may lead to differences in conclusions and warrants further investigation in future research.

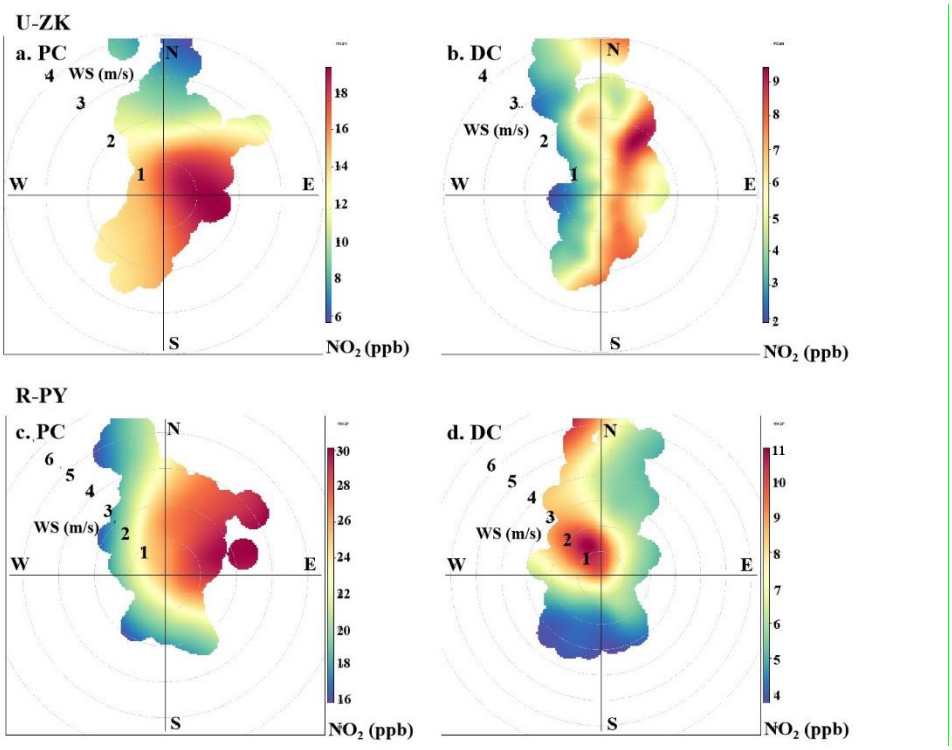

Figure S2. Result of conditional bivariate probability function plots: NO_2 at U-ZK and R-PY sites before (PC) and during (DC) the COVID-19 outbreak. The color scale bar represents NO_2 concentration.

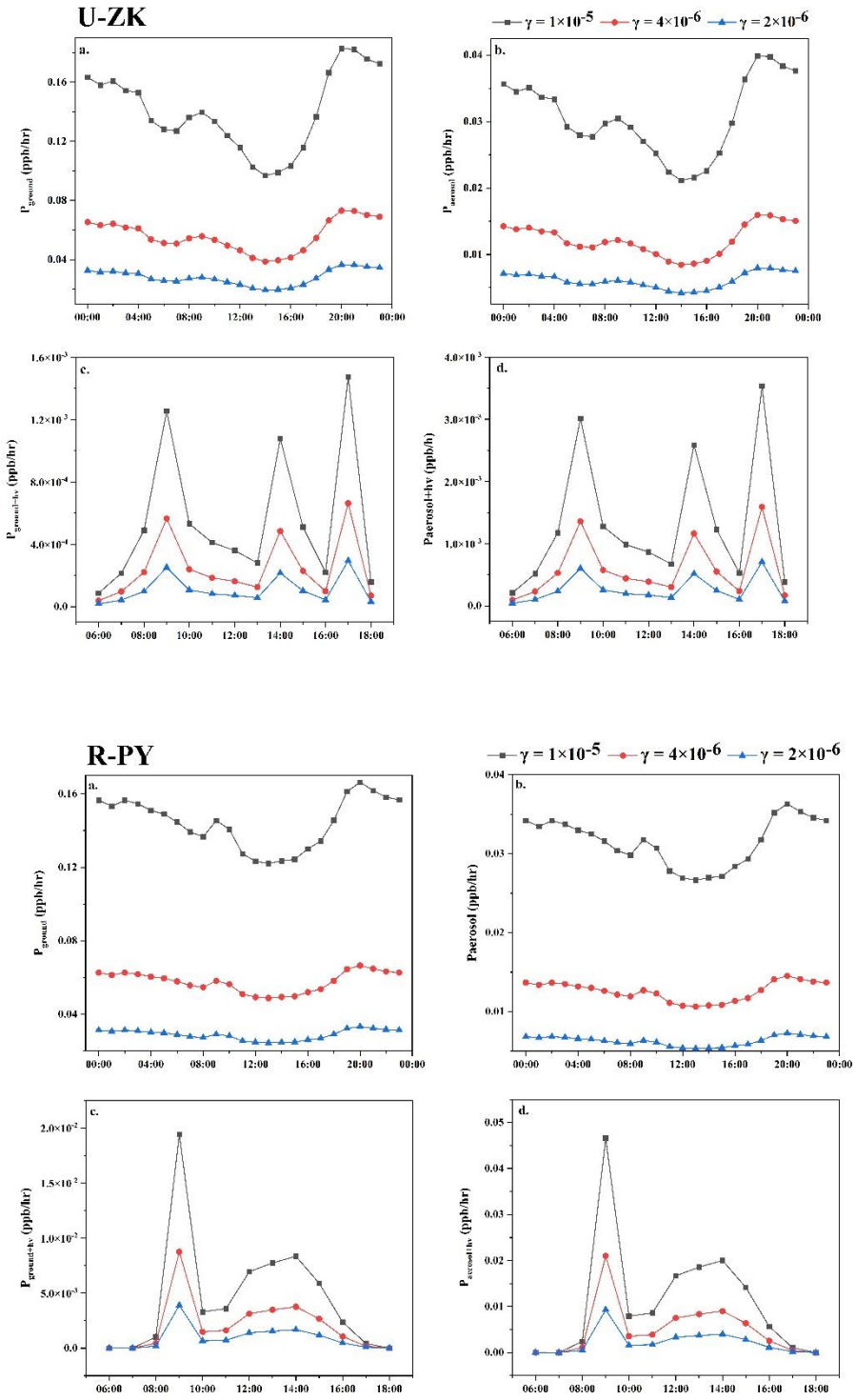

Figure S3. HONO production rate using different uptake rates of NO_2 at the U-ZK and R-PY sites before (PC) and during (DC) the COVID-19 outbreak. (a)P_{ground}, (b) $P_{aerosol}$, (c) $P_{ground+hv}$, and (d) $P_{aerosol+hv}$

Table S3. Summary of vehicle emission factors.

Observation site	Period	Emission factor (%)	Reference
Beijing	2020	0.79	(Meng et al., 2020)
Hong Kong	2015	0.4–1.8	(Yun et al., 2017)
Hong Kong	2011	0.5–1.6	(Xu et al., 2015)
Kiesberg Tunnel	2001	0.8	(Kleffmann et al., 2003)
Kiesberg Tunnel	1997	0.3–0.8	(Kurtenbach and Wiesen, 2001)
Guangzhou	2019	1.31	(Li et al., 2021b)

4. The uptake coefficient of NO_2 on surfaces is not mentioned.

Response: Thank you for your comment. We have added the description of the uptake coefficient of NO_2:

"γ_1 and γ_2 are the absorption coefficient of NO_2 on the ground and aerosol surface, respectively, which is assumed to be 4×10^{-6} (Yu et al., 2022; Zhang et al., 2021; Zhang et al., 2020a). Moreover, we discuss the uncertainties based on the recommended values of 2×10^{-6}–1×10^{-5} as upper and lower bounds(Chen et al., 2023; VandenBoer et al., 2013; Wong et al., 2011). Results show (Figure S3) that the uncertainties for P_{ground}, $P_{aerosol}$, $P_{groung+hv}$, and $P_{aerosol+hv}$ are −50% to 150%, −50% to 151%, −20% to 120%, and −50% to 121% at the U-ZK, respectively. At the R-PY, the uncertainties for P_{ground}, $P_{aerosol}$, $P_{groung+hv}$, and $P_{aerosol+hv}$ are −50% to 150%, −50% to 151%, −20% to 120%, and −50% to 121%, respectively."

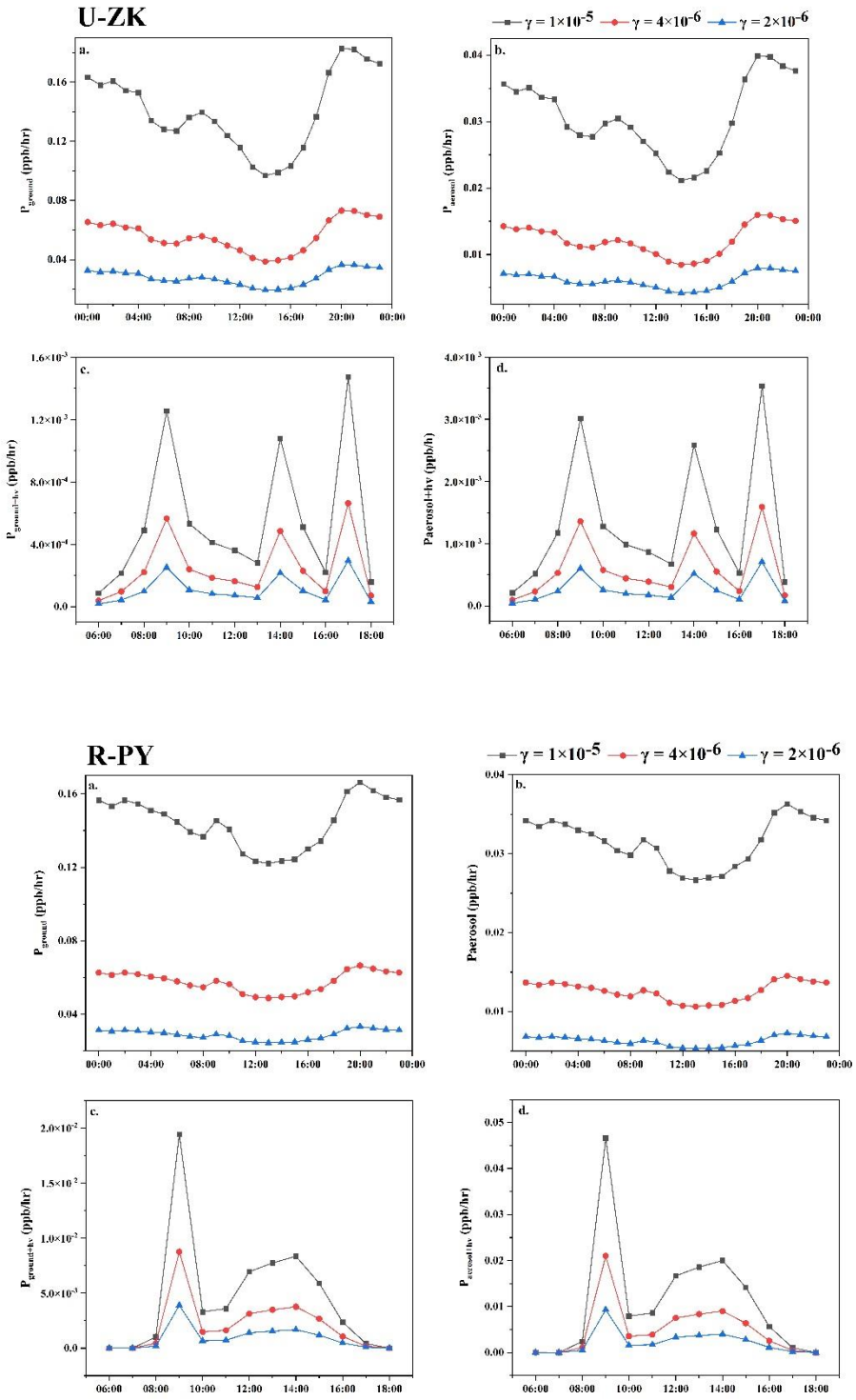

Figure S3. HONO production rate using different uptake rates of NO_2 at the U-ZK and R-PY sites before (PC) and during (DC) the COVID-19 outbreak. (a)P_{ground}, (b) $P_{aerosol}$, (c) $P_{ground+hv}$, and (d) $P_{aerosol+hv}$

5. The same OH concentration used at all station is also controversial.

Response: Thank you for your comments. We have modified the method for determining •OH concentration in the revised manuscript:

•OH concentration was simulated according to the empirical model (Hu et al., 2022; Wang et al., 2025):

$$[OH] = 4.1\times10^{9}\times\frac{J(O^{1}D)\times J(NO_2)\times(140\times[NO_2]+1)+[HONO]\times J(HONO)}{0.41\times[NO_2]^{2}+1.7\times[NO_2]+1+[NO]\times k_{NO+OH}+[HONO]\times k_{NO+OH}} \quad (3)$$

where, J (O^1 D), J (NO_2), and J (HONO) are the photolysis rates calculated using the TUV model (v5.2; available at http://cprm.acom.ucar.edu/Models/TUV/). The cloud optical depth value for the TUV model was adjusted so that the predicted UVB radiation intensity matched the observations (Lyu et al., 2019; Wang et al., 2022b). The calculated •OH concentration varied from 0.1 × 10^6 to 4 × 10^6 molecule/cm^3 at U-ZK and 0.1 × 10^6 to 5 × 10^6 molecule/cm^3 t R-PY, which was comparable to the levels in other cities of North China (Li et al., 2018; Fuchs et al., 2017; Yang et al., 2017). Since there is no photolysis at night, the •OH concentration was assumed to be 0.8 × 10^6 molecule/cm^3 (Wang et al., 2022).

6. In the supplement, is the equation (4) utilized in the calculation?

Response: Sorry for the mistake. We have corrected the formula:

$$P_{ground} = \frac{1}{8}\gamma_1\times[NO_2]\times C_{NO_2}\times\frac{S_g}{V} \quad (4)$$

$$P_{aerosol} = \frac{1}{4}\gamma_2\times[NO_2]\times C_{NO_2}\times\frac{S_a}{V} \quad (5)$$

$$\frac{S_g}{V} = \frac{1}{MLH} \quad (6)$$

7. The J_{HONO} and $J_{nitrate}$ used are suggested to be described in detail.

Response: Thanks for your suggestion. We have added a detailed description:

"$J(O^1D)$, $J(NO_2)$, and J(HONO) are the photolysis rates calculated using the TUV model (v5.2; available at http://cprm.acom.ucar.edu/Models/TUV/). The cloud optical depth value for the TUV model was adjusted so that the predicted UVB radiation intensity matched the observations (Lyu et al., 2019; Wang et al., 2022b)."

"The $J_{nitrate \rightarrow HONO}$ was simulated by normalizing UV values when the Zenit Angle is 0°, $J_{nitrate \rightarrow HONO}$ varied within the range of 1.22×10^{-5} to 4.84×10^{-4} s^{-1}, with an average value of 8.24×10^{-5} s^{-1} (Bao et al., 2018)."